Monitoring the crystallization process of a zeolite structure on SBA-15 mesopore walls

Sami Habib,[a] Franck Launay,*[a] Marie-Anne Springuel-Huet,[a] Flavien Guenneau,[a] Virginie Semmer-Herlédan,[a] Nataša Novak Tušar,[b] Venčeslav Kaučič[b] and Antoine Gédéon*[a]

Received (in Montpellier, France) 14th March 2006, Accepted 2nd June 2006
First published as an Advance Article on the web 20th June 2006
DOI: 10.1039/b603843c

Hierarchical materials based on crystallization of the MFI structure on mesoporous Al-SBA-15 have been synthesized by a hydrothermal procedure in water. The effect of the crystallization temperature and time as well as the proportion of zeolite template has been investigated. In addition to XRD, TEM and N_2 sorption measurements, the structural and textural properties of the materials have also been studied by hyperpolarized (HP) ^{129}Xe NMR and FTIR. These techniques emphasized that the main issue during the synthesis procedure is to find the optimal parameters (time, temperature and concentrations) in order to maintain the structure of the Al-SBA-15 mesoporous solids under the conditions required for zeolite crystallization. Embryonal MFI crystals have been identified on SBA-15 walls which remained ordered for materials obtained with TPABr : Al molar ratio of 0.7 : 1 after 8 h of hydrothermal treatment at 180 °C. Evidence for these zeolite nanocrystals has been obtained for the first time by hyperpolarized ^{129}Xe NMR spectroscopy. Moreover, this was corroborated by the appearance of an IR absorption band at 542 cm^{-1} due to the asymmetric stretching vibration of the double five-membered rings present in ZSM-5.

Introduction

Microporous molecular sieves which possess a high surface area, an adjustable pore size, high thermal and chemical stability, such as zeolites, are among the most widely used heterogeneous catalysts.[1] However, due to the limited size of their pores (<1.0 nm), zeolites cannot be applied for conversion of molecules with diameters larger than 1.0 nm.[2] It was expected that mesoporous molecular sieves (MCM-41,[3] SBA-15[4]) characterized by an ordered arrangement of pores and diameters of 2.0 to 10 nm could be suitable for the conversion of bulky molecules. However, mesoporous aluminosilica materials, such as Al-MCM-41[5] or Al-SBA-15[6] are less acidic, less catalytically active and less stable[7] than microporous zeolites.

It is thus very attractive to design new materials which combine the advantages of both mesoporous molecular sieves and zeolites. Different strategies have been used to generate hierarchical materials based on ZSM-5. To meet this goal, a generally applied method is the "intracrystalline" approach in which mesopores are created in the zeolite crystals most frequently *via* steaming and acid leaching[8] or by using secondary carbon templates.[9] The "intercrystalline" method is another way which consists in assembling ZSM-5 materials into ordered mesoporous structures. Such a concept is illustrated by the combination of a ZSM-5 molecular organic template, *i.e.* the tetrapropylammonium cation (TPA^+), with supramolecular templates of MCM-41[10–11] and MCM-48.[12] Recrystallization of ZSM-5 zeolites partially dissolved in an alkaline medium has also been tested.[13–14] Another "intercrystalline" synthesis route is based on the use of preformed mesoporous solids as starting materials. Their amorphous walls can be coated with the gel for ZSM-5 synthesis[15–16] or converted into a crystalline material by post assembly treatment with the appropriate template (zeolitization procedure).

Kloestra *et al.*[17] were the first to report the formation of tectosilicates/MCM-41 with high catalytic activity. The heterogeneous nucleation of embryonal ZSM-5 onto the surface of calcined Al-MCM-41 was obtained by exchanging protons with TPA^+ cations. Crystallization of the zeolite precursors was performed in glycerol at 120 °C in contrast to the procedure for synthesis described by Do and Kaliaguine which involved a hydrothermal treatment of MSU-1 and KIT-1 solids in the presence of small amounts of water.[18] Similar work on SBA-15 type solids has been described more recently by Campos *et al.*[19,20] The starting materials were either aluminosilicas with a high Si : Al molar ratio or pure silica combined with an external source of aluminium, both mesoporous samples being prepared under reflux conditions. The near absence of ZSM-5 or of its precursors[19] in the composite samples was explained by the low H^+/TPA^+ exchange capacity of the Al-SBA-15 solids. In contrast, pure silica SBA-15 impregnated by TPAOH and hydrothermally treated in a water–glycerol mixture at 120 °C gave rise to ZSM-5 whose presence was suggested using FTIR. For a longer

[a] *Université Pierre et Marie Curie - Paris 6, CNRS-UMR 7142, Laboratoire Systèmes Interfaciaux à l'Echelle Nanométrique, case 196, 4 place Jussieu, Paris F-75252 Cedex 05, France. E-mail: franck.launay@upmc.fr. E-mail: antoine.gedeon@upmc.fr; Fax: +33-1-4427-5536; Tel: +33-1-4427-7143*
[b] *National Institute of Chemistry, Hajdrihova 19, 1000 Ljubljana, Slovenia*

hydrothermal treatment, separate ZSM-5 particles were clearly shown by TEM and XRD.[20] Alternatively, a non-alkaline synthesis pathway based on the use of fluoride ions and TPABr failed due to the collapse of the mesopore structure. In this paper, we present a careful report on the crystallization process of the ZSM-5 structure on Al-SBA-15 solids with a high aluminium content. The effects of the hydrothermal temperature, the crystallization time and the relative amounts of ZSM-5 precursors have been studied. XRD and TEM measurements coupled to spectroscopic analyses (FTIR and HP ^{129}Xe NMR) gave reasonable evidence of ZSM-5 crystallite formation on a well-structured mesoporous framework. The catalytic activity of the materials was tested in the acid-catalyzed condensation of 2-methylfurane and acetone.

Experimental

Synthesis of Al-SBA (OP) ("one-pot")

Al-SBA (OP) was obtained according to the method described by Li *et al.*,[21] using Pluronic P123 ($EO_{20}PO_{70}EO_{20}$, Aldrich) as the structure directing agent, tetramethyl orthosilicate (TMOS, Fluka) and aluminium isopropoxide (Acros) as the silicon and aluminium precursors, respectively. Al-SBA-15 was synthesized by dissolving 4 g of Pluronic P123 in 150 mL of aqueous HCl at pH = 1.5 (solution "A"). Then, 6.4 mL of TMOS and 0.88 g of aluminium isopropoxide were added to 10 mL of aqueous HCl at pH = 1.5 (solution "B"). Solution "B" was stirred at room temperature for about 3 h and then added dropwise to solution "A". The resulting mixture was aged for 20 h at 40 °C and then transferred into an autoclave at 100 °C for 24 h. The as-synthesized solid (as-Al-SBA (OP)) (Si : Al = 17 : 1) was collected by filtration, washed with water and dried at 60 °C for 15 h. Finally, the surfactant was removed by calcination under flowing air (9 L h^{-1}) at 550 °C for 8 h (24 °C h^{-1}).

Transformation of the amorphous walls of mesoporous Al-SBA-15 (OP) (Si : Al = 17 : 1)

As-synthesized or calcined Al-SBA (OP) samples (0.5 g) were impregnated with 2 mL of an aqueous solution of TPABr (0.40 or 0.08 g, Aldrich) and NH_4F (0.25 or 0.05 g, Fluka) for 1 h. Most of the water was removed under vacuum and the solid was further dried at 60 °C for 24 h. The obtained material was again suspended in water (10 mL) and the pH adjusted to 9 or 10 using 0.04 or 0.1 M NaOH solutions, respectively. The resulting mixture was stirred overnight at room temperature and treated hydrothermally (130 or 180 °C) for different times (2, 8, 16 or 24 h). The solid was recovered by centrifugation, washed with distilled water, centrifuged again and subsequently dried overnight at room temperature followed by 2 h at 100 °C. Finally, the solid was calcined in flowing air at 550 °C for 6 h.

Characterization

The different solids were characterized by X-ray diffraction on a BRUKER D8 ADVANCED diffractometer using Cu-Kα radiation in the range between 0.5° and 5° (2θ) (low-angle XRD) and between 5° and 50° (2θ) (high-angle XRD). Nitrogen sorption experiments were carried out at −196 °C on a Micromeritics ASAP 2010 apparatus. Prior to the analysis, samples were outgassed at 200 °C overnight. The specific surface areas were evaluated using the Brunauer–Emmett–Teller (BET) method in the P/P_0 range of 0.05–0.3. Pore size distribution curves were calculated from the desorption branch of the N_2 isotherms using the Barrett–Joyner–Halenda (BJH) method. Transmission electron microscopy studies were performed on a JEM-100 CX electron microscope (JEOL, Japan). Prior to measurement, samples were deposited as ethanol suspensions on a grid of holey carbon film, dried and rapidly transferred to the microscope operating at 100 kV. Elemental analyses were performed by ICPAES (CNRS Analysis Centre, Vernaison, France) and by energy dispersive X-ray spectroscopy (EDXS) using a JEOL-2010F HRTEM 200 kV field-emission microscope equipped with a Si(Li) detector (LINK ISIS 300, Oxford Instruments) (National Institute of Chemistry, Ljubljana, Slovenia). Transmission infrared spectra were recorded on a BRUKER FTIR Vector 22 spectrometer using the KBr pellet technique. Prior to the xenon NMR measurements, samples were compressed at 40 MPa, placed in an NMR tube with two "Young" valves and evacuated at 400 °C overnight. Room temperature ^{129}Xe NMR spectra were collected on a Bruker DSX 300 spectrometer operating at 83.03 MHz. Hyperpolarized (HP) xenon was produced in the optical pumping cell in the fringe field of the spectrometer magnet. The Xe–He mixtures containing 8–1000 Torr of Xe polarized to *ca.* 1% were delivered at a 100 mL min^{-1} flow rate to the samples *via* plastic tubing. 64–256 FIDs were accumulated with 10 μs ($\pi/2$) pulses and 5 s repetition delays.

Catalysis tests

Samples were used as catalysts in the synthesis of 2,2-bis (5-methylfuryl)propane (DMP). 1.8 g of 2-methylfurane (MF) and 3.2 g of acetone were added to the solid catalyst. Undecane (100 μL) was subsequently introduced as an internal standard. The reaction mixture was stirred for 24 h at 50 °C. Finally, the solid was separated by centrifugation and the supernatant liquid was analyzed using a Delsi Nermag DN 200 gas chromatograph equipped with a SPB™-5 column and a FID detector. ZSM-5, Al-SBA (OP) and the new materials were compared to a commercial Nafion-H® silica composite, SAC-13® (1.04×10^{-4} mol SO_3H g^{-1}, Aldrich).

Results and discussion

Characterization of the starting Al-SBA (OP) material

The starting material Al-SBA (OP) was fully characterized in its calcined form. Hence, the regular hexagonal array of mesopores was shown through the presence of the three XRD peaks corresponding to the (100), (110) and (200) planes. Furthermore, nitrogen sorption isotherms of type IV with an H1 hysteresis loop were obtained.[22] They are consistent with a narrow pore size distribution centred on 8.0 nm. The surface area and porous volume was 790 m^2 g^{-1} and 1.1 cm^3 g^{-1}, respectively. Aluminium insertion through the co-condensation technique was partial (Si : Al = 17 : 1 instead of 10 : 1).

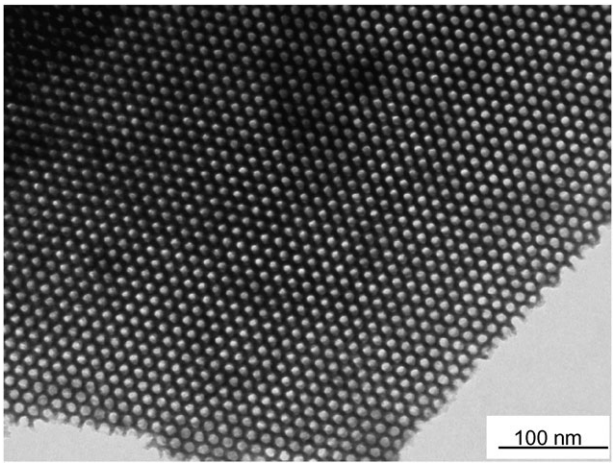

Fig. 1 TEM image of calcined Al-SBA(OP) (Si : Al = 17 : 1).

TEM images of calcined Al-SBA (OP) confirm well-ordered hexagonal arrays of mesopores with one-dimensional channels indicating a 2-D hexagonal (*P6mm*) mesostructure (Fig. 1). The distance between two consecutive centres of pores estimated from the TEM images is 13.0 nm, in agreement with the XRD patterns (12.9 nm).

Monitoring the transformation of as-synthesized Al-SBA-15 samples

The preparation procedure is based on three steps. First, the solid Al-SBA (OP) is impregnated with an aqueous mixture of the zeolite template (TPABr) and ammonium fluoride (step 1). After drying, the material is suspended in aqueous NaOH at pH = 9 or 10 for 12 h (step 2) in order to get seeds of zeolite. Last, the resulting mixture is treated hydrothermally (step 3). In order to better understand and to control the mechanism of zeolite crystallization, three parameters were varied: the hydrothermal treatment time, the crystallization temperature and the calcination. First experiments were performed on native Al-SBA (OP) samples at a typical crystallization temperature for ZSM-5 zeolites (T = 180 °C).[23,24] The hydrothermal treatment time (t) was varied between 2 and 24 h (Table 1). The composite samples are denoted OP-Z-$T(t)$. These materials were characterized by XRD either in their native or calcined form.

Low-angle XRD patterns of the samples are given in Fig. 2. In the case of OP-Z-180(2), the peak attributed to the (100) plane reflection is still observed but those due to (110) and (200) have disappeared, which indicates that some order remains in the pore structure. However, the absence of XRD reflections at high-angle confirms that microporous ZSM-5 is not formed under the above conditions (Fig. 3). As the crystallization time increases, the intensity of the low-angle peak strongly decreases indicating the collapse of the mesoporous structure (Fig. 2). The high-angle XRD patterns of OP-Z-180(24) (shown in Fig. 3) are very similar to those of the ZSM-5 (Si : Al = 23 : 1) prepared according to the procedure described in ref. 23. This confirms the occurrence of zeolite crystallization under these conditions. However, even for smaller hydrothermal treatment times, the appearance of poorly-resolved signals (around 8–10° (2θ) for OP-Z-180(8)) could reflect the formation of embryonal zeolite crystals.

Table 1 Synthesis conditions and experimental Si : Al ratio of composite materials

Materials	Crystallization time/h	Temperature/°C	Molar Si : Al ratio
OP-Z-180(2)	2	170	145 : 1
OP-Z-180(8)	8	180	170 : 1
OP-Z-180(16)	16	180	196 : 1
OP-Z-180(24)	24	180	31 : 1
OP-Z-130(24)	24	130[a]	114 : 1

[a] Uncalcined sample.

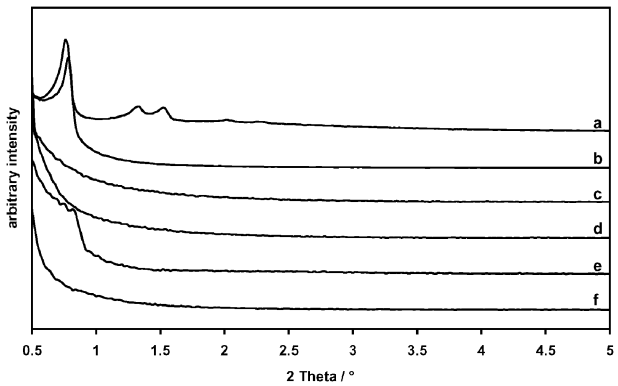

Fig. 2 Low-angle X-ray diffraction patterns of (a) Al-SBA (OP) (Si : Al = 17 : 1), (b) OP-Z-180(2), (c) OP-Z-180(8), (d) OP-Z-180(16), (e) OP-Z-180(24) and (f) uncalcined OP-Z-180(24).

In the absence of clear XRD evidence for ZSM-5 formation, the existence of very small crystals of zeolite can be proved by spectroscopic techniques such as ^{129}Xe NMR,[16] or FTIR.[12,17,25] When xenon is adsorbed in a porous system, the chemical shift can be simply expressed by the relation: $\delta = \delta_s + \delta_{Xe-Xe}$. The δ_s term arises from interactions between xenon atoms and the "solid walls". The δ_{Xe-Xe} term, due to Xe–Xe collisions, is pressure dependent in microporous systems but negligible for solids with large pores.[26] The spectrum

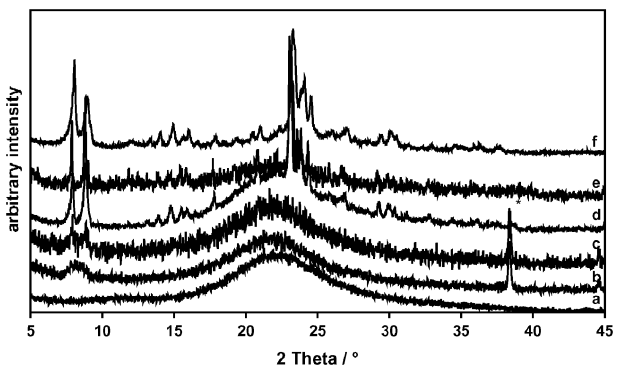

Fig. 3 High-angle X-ray diffraction patterns of (a) OP-Z-180(2), (b) OP-Z-180(8), (c) OP-Z-180(16), (d) OP-Z-180(24), (e) uncalcined OP-Z-180(24) and (f) ZSM-5 (Si : Al = 23 : 1). (*) Diffraction peak due to Al of the sample holder.

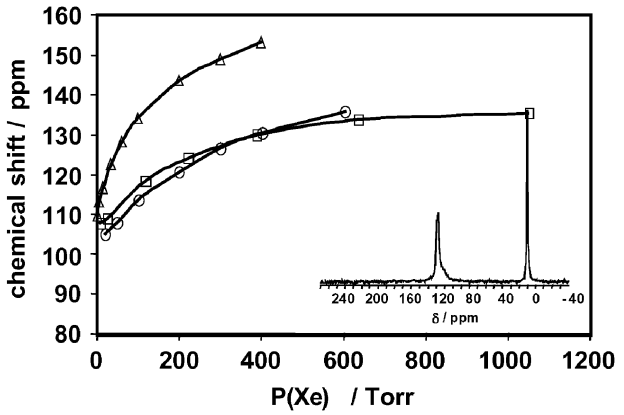

Fig. 4 Chemical shift (ppm) *versus* xenon pressure (Torr) for OP-Z-180(16) (□), ZSM-5 (Si : Al = 18 : 1) (△) and silicalite (○). Inset: HP ^{129}Xe NMR spectrum of OP-Z-180(16) recorded under 9 Torr Xe pressure.

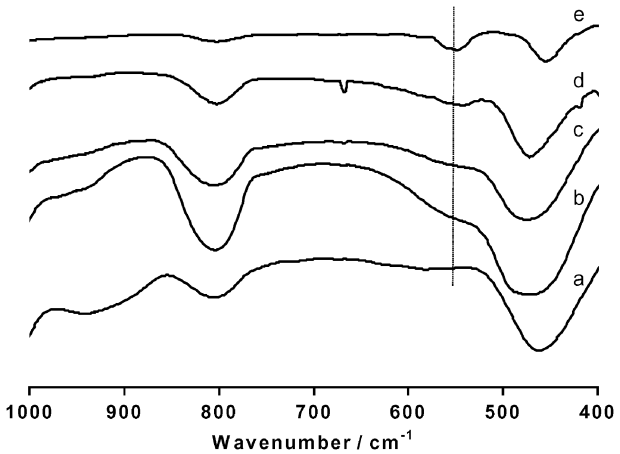

Fig. 5 IR spectra of (a) Al-SBA (OP), (b) OP-Z-180(8), (c) OP-Z-180(16), (d) OP-Z-180(24), and (e) ZSM-5 (Si : Al = 23 : 1).

of xenon adsorbed at room temperature on OP-Z-180(16) contains one line corresponding to adsorbed xenon (inset in Fig. 4) in addition to the gas phase signal. Fig. 4 shows the HP ^{129}Xe NMR chemical shift variation *versus* the equilibrium xenon pressure in OP-Z-180(16). For comparison, chemical shift variations for ZSM-5 (Si : Al = 18 : 1) and silicalite zeolites have been added. The increase in the chemical shift with Xe pressure proves that micropores of zeolitic type are present in OP-Z-180(16). This is not the case for SBA-15 materials (with no micropores in the walls) where the chemical shift slightly decreases when the xenon pressure increases.[27] The value extrapolated at zero pressure, δ_s, of the composite sample (108 ppm), is similar to those obtained for silicalite (102 ppm) and ZSM-5 zeolites (109 ppm).[28] Such a value, due to the Xe–wall collisions only, reflects the MFI structure of the porous OP-Z-180(16) material where xenon is adsorbed. The slight difference between the obtained δ_s values might be due to the aluminium content in the material.[28–30] Indeed, δ_s increases from 102.3 ppm to 110.8 ppm when Si : Al ratio decreases from 1950 : 1 to 24 : 1.[28] The similarity of the $\delta = f(P_{Xe})$ variations for the silicalite zeolite and OP-Z-180(16) provides additional evidence for the presence of the MFI structure. Despite a similar Si : Al ratio, the chemical shifts for OP-Z-180(16) are smaller than those of the ZSM-5 sample whatever the xenon pressure. This might be due to the fast exchange process which occurs between xenon gas phase ($\delta_{gas} = 0$) and xenon adsorbed in the zeolite framework. The smaller the crystal size, the greater is the exchange. This is compatible with the presence of embryonal ZSM-5 crystals in the OP-Z-180(16) material.

Fig. 5 shows the FTIR spectra of composite samples with different crystallization times. All the materials exhibit bands at 450 and 800 cm^{-1} due to the T–O bending vibration of the SiO_4 and AlO_4 internal tetrahedra and symmetric stretching vibrations of the internal and external Si–O–T linkage.[25] The band at 542 cm^{-1} which corresponds to the asymmetric stretching vibration of the double five-membered rings present in ZSM-5 (Si : Al = 23 : 1) is not observed in the spectrum of Al-SBA-15 (Si : Al = 17 : 1). In contrast, a shoulder whose intensity increases with the crystallization time appears at a similar wavenumber for the OP-Z-$T(t)$ materials. These results are in agreement with the formation of embryonal ZSM-5 structures.[16,25] Furthermore, the ratio (A : B) of the intensities of the peaks at 542 (A) and 450 cm^{-1} (B) has been used to estimate the crystallinity of ZSM-5. The highest ratio is logically found for the sample OP-Z-180(24) which contains segregated zeolite particles.

The collapse of the mesoporous structure during the crystallization process is clearly emphasized by the evolution of the N_2 sorption isotherms (*vide infra*). We have also checked that the removal of the template by calcination is not responsible for the observed destruction of the hexagonal arrangement of mesopores observed. The uncalcined OP-Z-180(24) sample contains zeolitic materials but displays no order in the 0–5° 2θ range. Similarities between calcined and native OP-Z-180(24) samples mean that, so far, the time and/or the crystallization temperature are the main factors controlling the structural mesopore stability. Zeolites like ZSM-5 can also be synthesized under milder conditions.[31] That is why another set of conditions based on a lower crystallization temperature (130 °C) was tested in order to preserve the structure of the mesoporous precursor. The solid OP-Z-130(24) is not structured at all according to XRD data (not shown). From this

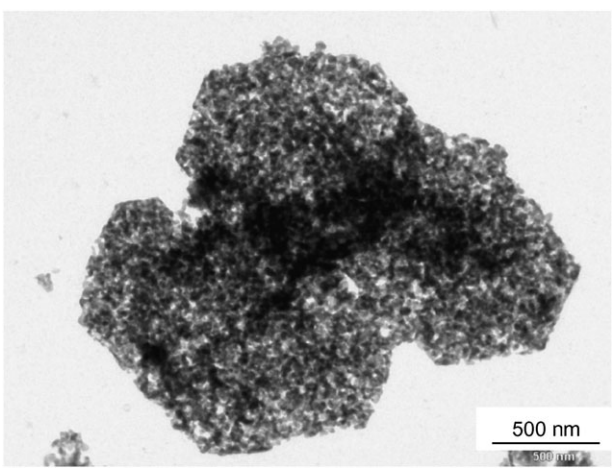

Fig. 6 TEM image of the hexagonal particles in OP-Z-180(2).

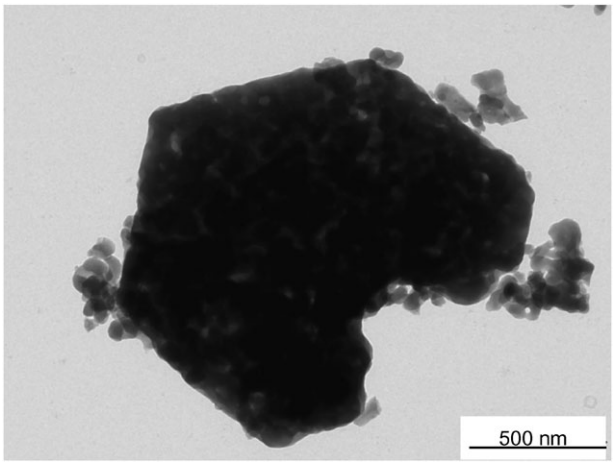

Fig. 7 TEM image of OP-Z-180(24).

result, it is clear that the hydrothermal treatment needs to be run at a higher temperature for a shorter crystallization time.

Elemental analyses of the samples Al-SBA (OP) and OP-Z-*T*(*t*) are summarized in Table 1. All solids contain less aluminium than the parent Al-SBA (OP). The loss of aluminium depends on the synthesis conditions. It appears that the molar Si : Al ratio of OP-Z-180(24), *i.e.* the most crystalline sample, is close to that of the starting Al-SBA-15. It is possible that the treatment of the solids by NaOH and NH_4F leads to a selective dissolution of Al species. We think that these are lost during the filtration procedure.

Transmission electron micrographs of the two extreme samples of the series, OP-Z-180(2) (Fig. 6) and OP-Z-180(24) (Fig. 7 and 8), are compared with those of their precursor Al-SBA (OP) (Si :Al = 17 : 1) (Fig. 1).

Both composite samples are clearly not homogeneous in comparison with Al-SBA-15. Hence, OP-Z-180(2) is constituted by hexagonal particles and a lot of small fragments (not shown here). It has to be noted that their amount is reduced in OP-Z-180(24). Particles in the OP-Z-180(2) and OP-Z-180(24) samples (Fig. 6 and 7) keep their hexagonal section, but their inner parts are strongly modified. Pores in the OP-Z-180(2) and OP-Z-180(24) samples are not regularly distributed which is in agreement with XRD data (Fig. 2). Irregular pore diameters of roughly 12.0 nm can be observed in the hexagonal OP-Z-180(2) particles (Fig. 6). Furthermore, the porous volume of the OP-Z-180(24) material (Fig. 7) seems to be lower than that of OP-Z-180(2). Most of the pores in OP-Z-180(24) seem to be blocked by a kind of deposit. In this latter case, various crystals (roughly 0.6 × 5 μm) of ZSM-5 can be observed (Fig. 8). Their formation seems to be associated with the disappearance of the small fragments.

Elemental analyses reflect the overall aluminium content. TEM-EDX analyses of Al-SBA (OP) confirm that Al is regularly distributed in the solid (17 : 1 < molar Si : Al ratio < 19 : 1). In contrast to their parent sample, the composition of the OP-Z-180(2) and OP-Z-180(24) materials is inhomogeneous. The atomic percentage of aluminium is strongly reduced in the hexagonal particles (Fig. 6 and 7) remaining after NaOH, NH_4F and hydrothermal treatment. The loss of aluminium is more pronounced in OP-Z-180(24) (Si : Al > 1500 : 1, Fig. 7) than in OP-Z-180(2) (300 : 1 < Si : Al < 800 : 1, Fig. 6). Most of the aluminium atoms in OP-Z-180(24) are located in the zeolite crystals (Si : Al = 47 : 1, Fig. 8).

Nitrogen sorption isotherms (Fig. 9) are strongly modified after the different zeolitization treatments. The porous volumes (0.04–0.13 $cm^3\ g^{-1}$) and surface areas (39–90 $m^2\ g^{-1}$) are reduced in all the OP-Z-*T*(*t*) materials. Changes in the isotherm shapes from Al-SBA (OP) to OP-Z-180(2) and OP-Z-180(24) materials are in agreement with the formation of a microporous solid and the collapse of the mesopores as shown by XRD and TEM techniques. Hence, it is noteworthy that the N_2 adsorption isotherm of OP-Z-180(24) (see inset in Fig. 9) recorded on the automatic apparatus looks sigmoidal at very low pressure. Such an artefact is due to the slow release of He that is used to measure the dead space of the mannifold. It shows unambiguously that ultramicropores ($\varnothing$ < 1 nm) are present in accordance with the formation of zeolitic deposits.

True composite materials H-ZSM-5–Al-SBA-15 should be characterized by strong acidic sites and high diffusion properties like H-ZSM-5 zeolite and the mesoporous Al-SBA-15 precursor, respectively. Recently, arenesulfonic materials combining both properties were shown to exhibit much better activity than H-ZSM-5 and Al-SBA-15 in the liquid phase condensation of 2-methylfuran (MF) with acetone.[32]

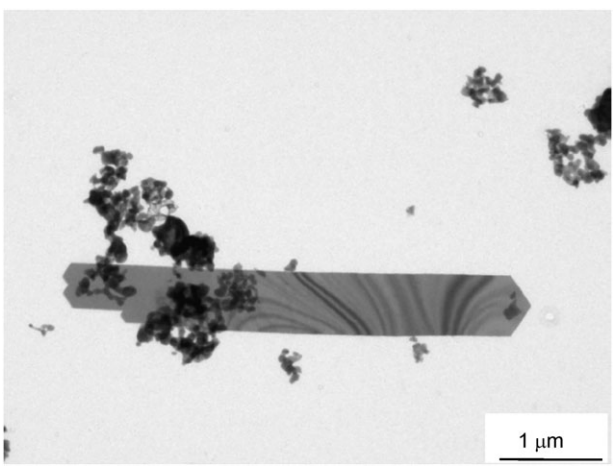

Fig. 8 TEM image of OP-Z-180(24).

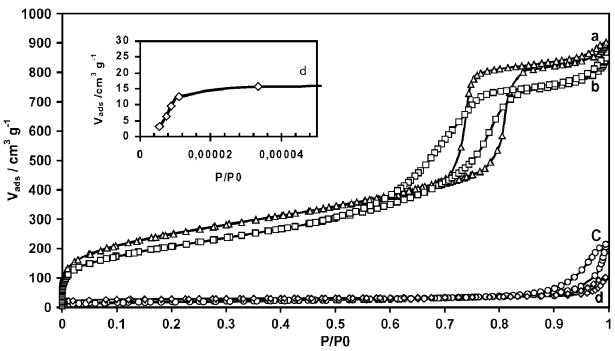

Fig. 9 Nitrogen sorption isotherms of (a) Al-SBA (OP) (Si : Al = 17 : 1), (b) as-Al-SBA (OP)–NaOH, (c) OP-Z-180(2) and (d) OP-Z-180(24). Inset: enlargement of the N_2 adsorption isotherm for sample OP-Z-180(24) at the lowest pressures.

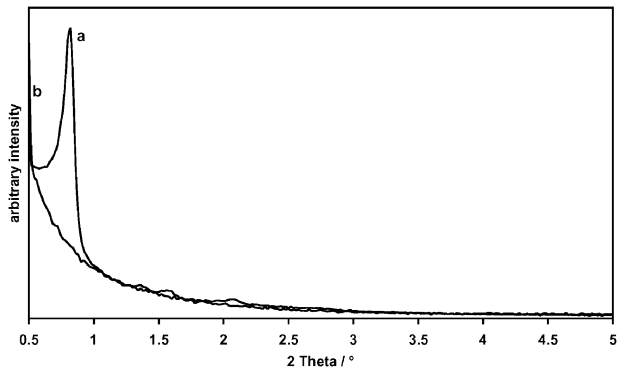

Fig. 10 Low-angle X-ray diffraction patterns of (a) OP-Z′-180(8) and (b) OP-Z-180(8).

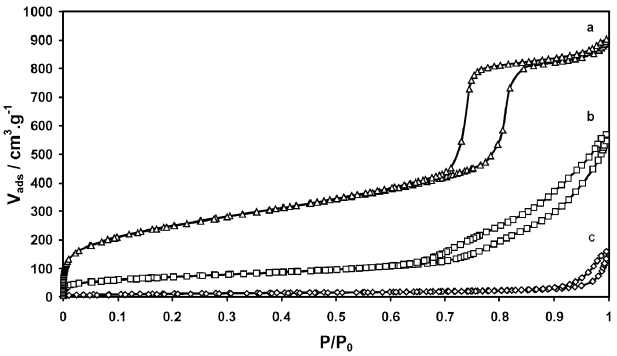

Fig. 12 Nitrogen sorption isotherms of (a) Al-SBA (OP) (Si : Al = 17 : 1), (b) OP-Z′-180(8) and (c) OP-Z-180(8).

Considering that similar results should be obtained with Al-containing composite solids displaying interconnection between their micropore and mesopore networks, the same test was performed in order to get more information on their structure. As expected from ^{129}Xe NMR and TEM data, catalysis tests carried out with OP-Z-180(2) and OP-Z-180(24) did not lead to better DMP yields (0.3%) than with H-ZSM-5 (0.4 to 2% for a MF : Al molar ratio between 1500 : 1 and 225 : 1) and Al-SBA (OP) (1.6 to 5.3% for a MF : Al molar ratio between 1500 : 1 and 225 : 1). Such results are in agreement with the textural properties of OP-Z-180(2) and OP-Z-180(24) as well as the segregation of zeolite particles. The commercial Nafion-H® silica composite, SAC-13®, used for the sake of comparison (MF : Al molar ratio of 1500 : 1) led to a 70% yield of DMP.

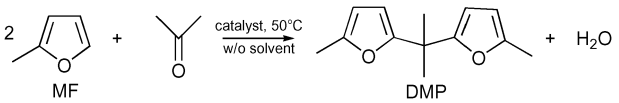

Given that the transformation of the mesopore walls into zeolitic materials is based on the alkaline treatment of the precursor, it was crucial to check the stability of Al-SBA-15 prior to the hydrothermal synthesis.[33] It turned out that the textural (V_p = 1.1 cm^3 g^{-1}, S = 754 m^2 g^{-1}, Fig. 9) and structural (not shown here) properties of the intermediate solid (as-Al-SBA (OP)–NaOH) are much more similar to those of the starting Al-SBA-15 than those of the OP-Z-180(2) and OP-Z-180(24) solids. It can be concluded that the hydrothermal treatment is mainly responsible for the destruction of the mesopores in Al-SBA (OP) observed during the zeolitization procedure. So far, the results show the difficulty in getting well-defined MFI-ZSM-5 crystallites and preserving at the same time the mesoporous framework. In addition to the effects of the temperature and the crystallization time, we investigated the influence of the reactant molar ratio used for the zeolite synthesis. Keeping constant the previous TPABr : Al and NH_4F : Al ratio, it was observed that lower amounts of NaOH (0.04 M instead of 0.1 M) did not help to preserve the mesoporous structure of the samples. On the other hand, a great improvement has been observed by dividing by five the amounts of TPABr and NH_4F and using 0.04 M sodium hydroxide (sample OP-Z′-180(8)). In contrast to OP-Z-180(8), the X-ray diffraction pattern of the sample treated hydrothermally for 8 h, OP-Z′-180(8) (Fig. 10), still exhibits typical peaks of the SBA-15 hexagonal array of mesopores.

The structure of the porous network is confirmed by TEM images of OP-Z′-180(8). Moreover, electron micrographs (Fig. 11) indicate that the material consists of hexagonal particles. However, it has to be noted that the contours of the particles and of the pores are less well-defined than in the Al-SBA (OP) solid.

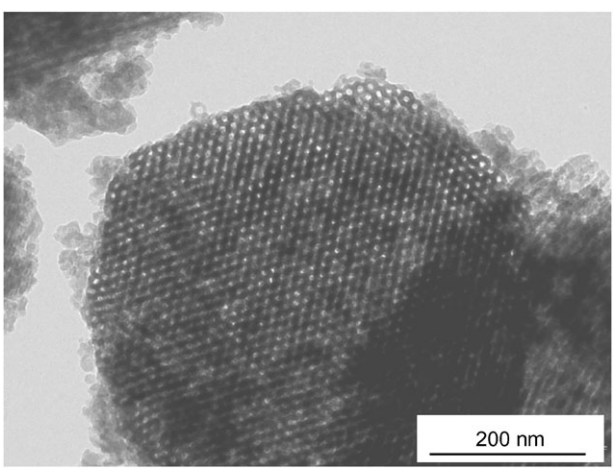

Fig. 11 TEM image of OP-Z′-180(8).

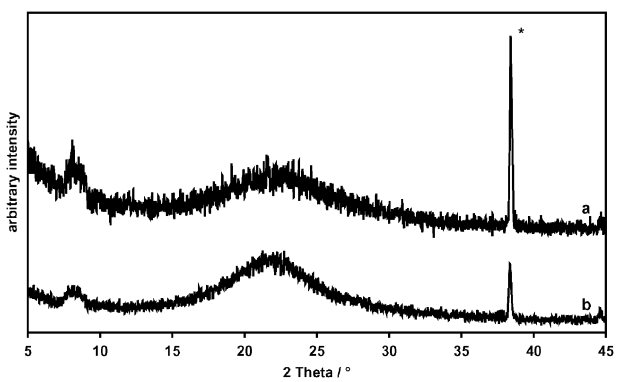

Fig. 13 High-angle X-ray diffraction patterns of (a) OP-Z′-180(8) and (b) OP-Z-180(8). (*) Diffraction peak due to Al of the sample holder.

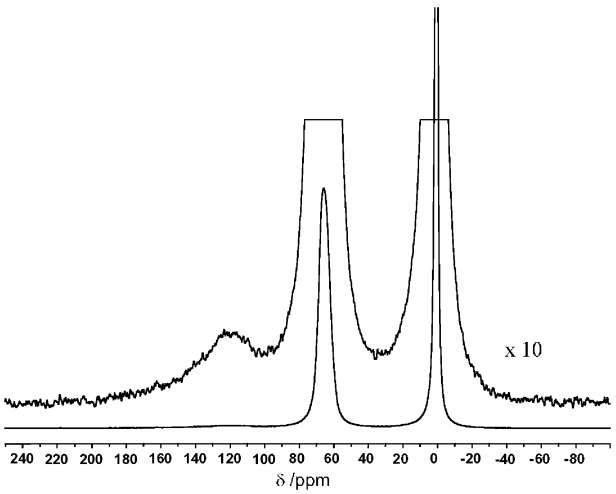

Fig. 14 HP ^{129}Xe NMR spectrum of OP-Z′-180(8).

Nitrogen sorption data of OP-Z′-180(8) (Fig. 12b) are consistent with the presence of mesopores with a large distribution compared to the starting material. Actually, the surface area and porous volume of OP-Z′-180(8) are 250 m^2 g^{-1} and 0.6 cm^3 g^{-1}, respectively which are much higher than those of the corresponding Z materials. Failing in the stabilization of the Al-SBA precursor, we have shown that its impregnation under smoother conditions, *i.e.* lower TPABr : Al and NH_4F : Al ratios is a determining parameter on the way to true composite materials. To the best of our knowledge, these results show for the first time that the mesoporosity can be maintained during the zeolitization process despite the aqueous nature of the medium. Accordingly, elemental analyses of OP-Z′-180(8) show that the loss of aluminium is severely reduced (Si : Al = 24 : 1) compared to OP-Z-180(8) (Si : Al = 170 : 1, Table 1). However, less template molecules give rise to lower amounts of ZSM-5 crystallites. As a matter of fact, high-angle X-ray diffraction is not very helpful to detect the MFI structure (Fig. 13).

Better evidence for the presence of zeolitic type micropores is brought by the HP ^{129}Xe NMR spectrum (Fig. 14). In contrast to OP-Z-180(16) (inset in Fig. 4), two signals are observed at 70 and 120 ppm besides Xe gas (δ = 0 ppm). The most intense peak (70 ppm) was attributed to Xe located in the mesopores whereas the other (120 ppm) corresponds to ZSM-5 crystallites.

Conclusion

We first demonstrated that the crystallization of the ZSM-5 structure on Al-SBA-15 mesoporous materials can be successfully obtained by a hydrothermal procedure in aqueous medium. Optimal synthesis conditions have been achieved by varying the hydrothermal treatment time and temperature. After 8 h at 180 °C, embryonal MFI zeolite crystals have been obtained. Moreover, reducing the TPABr : Al ratio, under these conditions, allows preservation of the initial mesopore structure.

HP ^{129}Xe NMR and FTIR spectroscopies combined with preliminary results of catalysis tests have been used to investigate the presence of zeolite nanocrystals on the mesoporous aluminosilicate composites. In this paper, we have shown that hyperpolarized ^{129}Xe NMR is an ideal means for probing the MFI type of micropores and indirectly the very small size of zeolite particles. Experiments are in progress in order to investigate the intimacy of the microporous and mesoporous networks.

References

1 K. P. de Jong, *Catal. Rev. Sci. Eng.*, 2001, **45**, 297.
2 A. Corma, *Chem. Rev.*, 1995, **95**, 559.
3 J. S. Beck, J. C. Vortuli, W. H. Roth, M. E. Leonowicz, C. T. Kresge, K. D. Schmitt, C. T. W. Chu, D. H. Olson, E. W. Sheppard, S. B. McCullen, J. B. Higgins and J. L. Schlenker, *J. Am. Chem. Soc.*, 1992, **114**, 10834.
4 D. Zhao, J. Feng, Q. Huo, N. Melosh, G. H. Fredrickson, B. F. Chmelka and G. D. Stucky, *Science*, 1998, **279**, 548.
5 C. T. Kresge, M. E. Leonowicz, W. J. Roth, J. C. Vortuli and J. S. Beck, *Nature*, 1992, **359**, 710.
6 (*a*) S. Zeng, J. Blanchard, M. Breysse, Y. Shi, X. Shu, H. Nie and D. Li, *Microporous Mesoporous Mater.*, 2005, **85**, 297; (*b*) A. Vinu, G. Satish Kumar, K. Ariga and V. Murugesan, *J. Mol. Catal. A: Chem.*, 2005, **231**, 57; (*c*) S. Wu, Y. Han, Y. C. Zou, J. W. Song, L. Zhao, Y. Di, S. Z. Liu and F. S. Xiao, *Chem. Mater.*, 2004, **16**, 486; (*d*) Y. Yue, A. Gédéon, J. L. Bonardet, J. B. d'Espinose, J. Fraissard and N. Melosh, *Chem. Commun.*, 1999, 1967; (*e*) Z. Luan, M. Hartman, D. Zhao, W. Zhou and L. Kevan, *Chem. Mater.*, 1999, **11**, 1621.
7 A. Taguchi and F. Schüth, *Microporous Mesoporous Mater.*, 2005, **77**, 1.
8 A. Corma, *Chem. Rev.*, 1997, **97**, 2373.
9 A. Boisen, I. Schmidt, A. Carlsson, S. Dahl, M. Brorson and C. J. H. Jacobsen, *Chem. Commun.*, 2003, 958.
10 A. Karlsson, M. Stocker and R. Schmidt, *Microporous Mesoporous Mater.*, 1999, **27**, 181.
11 L. Huang, W. Guo, P. Deng, Z. Xue and Q. Li, *J. Phys. Chem. B*, 2000, **104**, 2817.
12 Y. Xia and R. Mokaya, *J. Mater. Chem.*, 2004, **14**, 863.
13 S. Inagaki, M. Ogura, T. Inami, Y. Sasaki, E. Kikuchi and M. Matsukata, *Microporous Mesoporous Mater.*, 2004, **74**, 163.
14 I. I. Ivanova, A. S. Kuznetsov, V. V. Yuschenko and E. E. Knyazeva, *Pure Appl. Chem.*, 2004, **76**, 1647.
15 T. O. Do and S. Kaliaguine, *J. Am. Chem. Soc.*, 2003, **125**, 618.
16 T. O. Do, A. Nossov, M. A. Springuel-Huet, C. Schneider, J. L. Bretherton, C. A. Fyfe and S. Kaliaguine, *J. Am. Chem. Soc.*, 2004, **126**, 14324.
17 K. R. Kloestra, H. V. Bekkum and J. C. Jansen, *Chem. Commun.*, 1997, 2281.
18 T. O. Do and S. Kaliaguine, *Angew. Chem., Int. Ed.*, 2001, **113**, 3348.
19 A. A. Campos, L. Martins, L. L. Oliveira, C. R. Silva, M. Wallau and E. Urquieta Gonzalez, *Catal. Today*, 2005, **107–108**, 759.
20 A. A. Campos, C. R. Silva, M. Wallau, L. D. Dinitrov and E. Urquieta Gonzalez, *Stud. Surf. Sci. Catal.*, 2005, **158**, 1581.
21 Y. Li, W. Zhang, L. Zhang, Q. Yang, Z. Wei, Z. Feng and C. Li, *J. Phys. Chem. B*, 2004, **108**, 9739.
22 *Adsorption, Surface Area and Porosity*, ed. S. J. Gregg and K. S. W. Sing, Academic Press, London, 2nd edn, 1982.
23 V. Gabova, J. Dedecek and J. Cejka, *Chem. Commun.*, 2003, 1196.
24 *Atlas of Verified Syntheses of Zeolitic Materials, Synthesis Commission of the International Zeolite Association*, ed. H. Robson and K. P. Lillerud, Elsevier, Amsterdam, 2001, p. 198.
25 R. Mohamed, H. Aly, M. El-Shahat and I. Ibrahim, *Microporous Mesoporous Mater.*, 2005, **79**, 7.
26 M. A. Springuel-Huet, J. L. Bonardet, A. Gédéon and J. Fraissard, *Magn. Reson. Chem.*, 1999, **37**, S1.
27 A. Nossov, E. Haddad, F. Guenneau, A. Galarneau, F. Di Renzo, F. Fajula and A. Gédéon, *J. Phys. Chem. B*, 2003, **107**, 12456.

28 Q. J. Chen, M. A. Springuel-Huet, J. Fraissard, M. L. Smith, D. R. Corbin and C. Dybowski, *J. Phys. Chem.*, 1992, **96**, 10914.
29 S. M. Alexander, J. M. Coddington and R. F. Howe, *Zeolites*, 1991, **11**, 368.
30 J. T. Timonen and T. T. Pakkanen, *Microporous Mater.*, 1997, **8**, 57.
31 (*a*) J. Aguado, D. P. Serrano, J. M. Escola and J. M. Rodriguez, *Microporous Mesoporous Mater.*, 2004, **75**, 41; (*b*) M. J. Eapen, S. V. Awate, P. N. Joshi, A. N. Kotasthane and V. P. Shiralkar, *Synthesis of Microporous Materials*, ed. L. M. Occelli and E. H. Robson, Van Nostrand Reinhold, New York, 1992, vol. 1, p. 139.
32 (*a*) W. M. Van Rhijn, D. E. De Vos, B. F. Sels, W. D. Bossaert and P. A. Jacobs, *Chem. Commun.*, 1998, 317; (*b*) D. J. Macquarrie, S. J. Tavener and M. A. Harmer, *Chem. Commun.*, 2005, 2363.
33 Y. Yue, A. Gedeon, J. L. Bonardet, N. Melosh, J. B. d'Espinose and J. Fraissard, *Stud. Surf. Sci. Catal.*, 2000, **129**, 209.

